

# Stereovision-based Integrated System for Point Cloud Reconstruction and Simulated Brain Shift Validation

Xiaochen Yang<sup>a</sup>, Logan W. Clements<sup>b</sup>, Ma Luo<sup>b</sup>, Saramati Narasimhan<sup>b</sup>, Reid C. Thompson<sup>c</sup>, Benoit M. Dawant<sup>a,b,d</sup>, Michael I. Miga<sup>b,c,d</sup>

<sup>a</sup>Vanderbilt University, Department of Electrical Engineering and Computer Science, Nashville, TN USA

<sup>b</sup>Vanderbilt University, Department of Biomedical Engineering, Nashville, TN USA

<sup>c</sup>Vanderbilt University Medical Center, Department of Neurological Surgery, Nashville, TN USA

<sup>d</sup>Vanderbilt University Medical Center, Department of Radiology, Nashville, TN USA

**Abstract.** Intra-operative soft tissue deformation, referred to as brain shift, compromises the application of current image-guided surgery (IGS) navigation systems in neurosurgery. A computational model driven by sparse data has been proposed as a cost-effective method to compensate for cortical surface and volumetric displacements. In this work, we present a mock environment developed to acquire stereo images from a tracked operating microscope and to reconstruct 3D point clouds from these images. A reconstruction error of 1 mm is estimated by using a phantom with a known geometry and independently measured deformation extent. The microscope is tracked via an attached tracking rigid body that facilitates the recording of the position of the microscope via a commercial optical tracking system as it moves during the procedure. Point clouds, reconstructed under different microscope positions, are registered into the same space to compute the feature displacements. Using our mock craniotomy device, realistic cortical deformations are generated. Our experimental results report approximately 2mm average displacement error compared with the optical tracking system. These results demonstrate the practicality of using tracked stereoscopic microscope as an alternative to LRS to collect sufficient intraoperative information for brain shift correction.

**Keywords:** Brain shift, stereoscopic microscope, intra-operative imaging, stereopsis, reconstruction, tracking, accuracy.

## 1 Introduction

Image-guided surgery (IGS) [1] provides a standard of care platform for guiding surgeons during brain tumor resection. Unfortunately, commercial IGS navigation systems do not have mechanisms to account for non-rigid tissue deformations which commonly arise from cerebrospinal fluid drainage, tissue swelling due to edema, tissue contraction due to hyperosmotic drugs, or tissue retraction/resection [2]. Solutions like intraoperative magnetic resonance (iMR) imaging [3], intraoperative computed tomography (iCT) [4], and intraoperative ultrasound (iUS) [5] have been proposed to compensate for soft-tissue changes. However, deficiencies like ionizing radiation of iCT, high cost of iMR, and poor image contrast/quality of iUS have compelled researchers to look for alternatives. Another cost effective method is to use sparse data acquired intraoperatively to

drive a biomechanical model to update and register preoperative images to the intraoperative field [6]. Laser range scanners (LRS) and stereoscopic microscopes are two widely used surface data acquisition techniques [7][8]. Both devices can be used in an operating room (OR) and generate three-dimensional cortical surface cloud data as well as a texture map. Typically, the microscope is continuously used during the whole surgery. Thus, it can provide high-resolution, consistent intraoperative information in near real-time with very limited interruption to the surgical workflow. Performing a single LRS acquisition is more disruptive because it takes about 15-30 seconds and requires the surgical microscope to be moved away from the surgical field of view. In recent work, we demonstrated using position-fixed stereo-pair cameras for surface measurements. This work used two identical Grasshopper digital cameras produced by Point Grey Research, Inc. (Richmond, British Columbia, Canada) and served as an initial testing prototype for our mock cortical surface environment [9].

In the work reported here, we have extended those approaches to a surgical microscope that is used clinically at our institution. We have developed an interactive environment that permits acquisition of stereo image capture from the microscope, calibration of the cameras, and adjustment of parameters used for 3D point cloud reconstruction. We have also equipped the microscope with a rigid body tracking star (MICROSCOPE TRACKING ARRAY, Brainlab Inc., Westchester, IL) to permit tracking of the microscope position within an IGS system. We show that with this device we can register 3D point clouds that are acquired with the microscope in different positions thus permitting an intraoperative calculation of cortical surface displacement. While the availability of microscope focal point tracking is possible with commercial IGS systems (although accuracy on these commercial systems is not widely reported), the implementation of a fully 3D tracked approach necessary for measuring full cortical surface field displacements is lacking.

## 2 METHODS

Section 2.1 describes the equipments used for data acquisition. Sections 2.2 and 2.3 explain the detail of stereovision techniques and integrated system, respectively. Section 2.4 shows the method of microscope tracking, and section 2.5 discusses the validation experiments.

### 2.1 Data acquisition

At Vanderbilt University Medical Center (VUMC) OPMI Pentero (Carl Zeiss, Inc., Oberkochen, Germany) surgical microscopes are routinely used during neurosurgery procedures (see Fig. 1 a). The scope used for this study is equipped with two charged-coupled device (CCD) cameras, Zeiss MediLive Trio, with a video frame rate of approximately 30 frames per second (FPS). The images or video stream in the field of view (FOV) can be displayed on a touchscreen monitor, controlled using a joystick, recorded, and exported by video output interface. Through an IEEE 1394 interface, captured data can be saved on a desktop or laptop. In our previous work, a user-friendly graphical user interface (GUI) was proposed to facilitate the acquisition and was designed to be compatible with all USB, Point Grey Research or other IEEE-1394b (FireWire) digital cameras [9] [10].

Our novel craniotomy simulation device is designed to permit in-plane stretching as well as out-of-plane deformation of a membrane to simulate realistic displacements occurring during surgery (see Fig. 1 c). Two circular rings inserts can be placed in the device aperture to simulate different craniotomy sizes which can vary substantially in different cases. Outside the main circle lie five hemispherical divots that are used for registration. Clamped by the four screws on each side of the device, the membrane inside the circle is made of Dragon Skin high performance silicone rubber and marked with a realistic mock cortical vessel pattern. Lateral shift can be simulated by

extending the right side of the device and stretching the silicon membrane through a lead-screw mechanism. In addition to lateral motion, the membrane can be pushed down more than 1 cm by four additional medium-size screws placed around the main circle, which indicates that brain sag often manifests as a withdrawal of the brain surface into the cranium on average of 1 cm although it depends on patient head orientation. Figure 1 d is a stair-block phantom that is used for calibration and verification experiment. At the center of each block, there is one red disc with a dent in the circle center which can be digitized by a tracked stylus. Other parts of the phantom are painted non-reflectively in order to improve the performance of disparity computing.

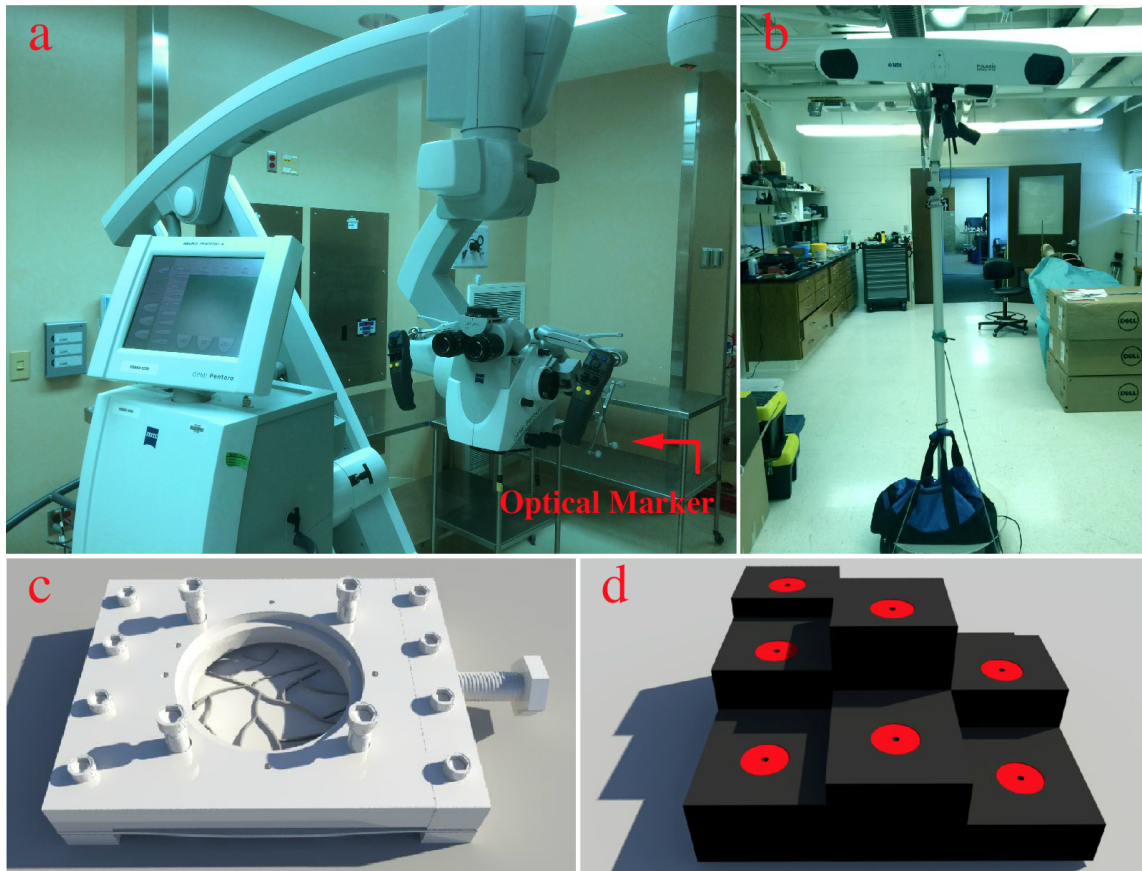


Fig 1: Surgical operating microscope with optical marker attached (a), optical tracking device (b), simulated craniotomy device (c), and calibration phantom (d)

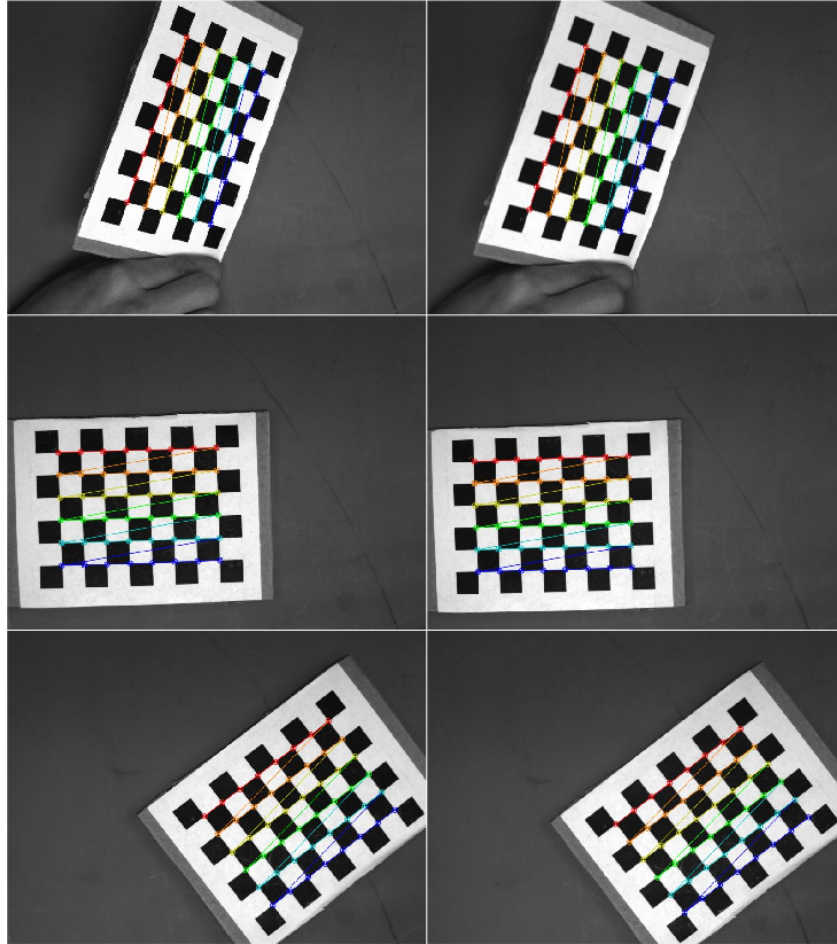


Fig 2: Three pairs of stereo images placed at different positions with corner detected

## 2.2 Stereovision

The first step in stereo calibration is capturing images of calibration objects. We use a planar chessboard pattern that has 8 x 6 internal corners with known size as shown in Fig. 2. The chessboard images need to be captured in different positions and orientations that cover the whole field of view. In order to determine both the intrinsic and extrinsic parameters of the stereo cameras, a process of calibration is needed to find the relationship between camera and world coordinate system. In our work, we rely on a classical and widely-used method [11] for camera calibration, which builds the epipolar geometry based on the pinhole model to search for corresponding points

in stereo matching. The fundamental matrix  $F$ , which encodes the epipolar geometry of two views, is defined by mapping a point in the left image  $x_1$  to its corresponding epipolar line  $l_2$  in the right image. For the corresponding point  $x_2$  in the right image lying on line  $l_2$ , the following equation is satisfied:

$$x_2^T F x_1 = 0 \quad (1)$$

The image pairs of the checkerboard pattern provide a number of correspondences which are used to solve  $F$  using a least squares method [11]. Then the camera matrix of each camera can be retrieved using the fundamental matrix  $F$ . The accuracy of calibration is evaluated by computing the distance between the corresponding corners and the estimated epipolar lines, since in theory the corresponding corner lies on the epipolar line.

The ultimate aim of the reconstruction process is to reproject 2D image points to physical world positions. The perspective reprojective matrix  $Q$  is defined below:

$$Q = \begin{bmatrix} 1 & 0 & 0 & -c_{x1} \\ 0 & 1 & 0 & -c_{y1} \\ 0 & 0 & 0 & f \\ 0 & 0 & -\frac{1}{T} & \frac{c_{x1}-c_{x2}}{T} \end{bmatrix} \quad (2)$$

where point  $(c_{x1}, c_{y1})$  is the principal point in left image,  $f$  is the focal length, and  $T$  is the horizontal distance between the two cameras centers  $C_1$  and  $C_2$ .  $c_{x2}$  is the x coordinate of the principal point in the right image. The bottom right corner  $(c_{x1} - c_{x2})/T$  is equal to zero if two principal rays intersect at infinity in a frontal parallel configuration. A 2D homogeneous point (associated

with disparity  $d$ ) can be transformed into a 3D point  $(X/W, Y/W, Z/W)$  in world space by the following mapping:

$$Q \begin{bmatrix} x \\ y \\ d \\ 1 \end{bmatrix} = \begin{bmatrix} X \\ Y \\ Z \\ W \end{bmatrix} \quad (3)$$

The image acquisition interface guarantees simultaneous capture of stereo pair, however, the left and right images are not perfectly parallel-aligned. Image pairs thus need to be rectified before computing disparity. Hartley et al. [12] have proposed an algorithm that find homographies that map the epipoles to infinity using just the fundamental matrix  $F$ . The main drawback of this method is the ambiguity in image scale, which can lead to inaccuracy in the size of the reconstructed 3D objects. Another algorithm has been proposed by Bouquet [13], which takes advantage of two calibrated cameras rotation and translation parameters to minimize reprojection distortions as well as maximizing the view overlap area. In this work, we have used Bouquet’s approach. After the rectification process is completed, the disparity map can be computed by finding the difference in  $x$  coordinates of the same features in the rectified left and right images. A number of algorithms have been proposed to calculate the disparity map, e.g., block matching (BM) [14], semi-global block matching (SGBM) [15], and a variety of other algorithms that have been evaluated and compared on an on-line platform [16] [17]. Considering simplicity, potential for near real time performance, and availability of open-source libraries such as Open Computer Vision Library (OpenCV)[18], we choose the BM approach for our stereo reconstruction algorithm. Most stereo matching algorithms are challenged by uniform texture-less areas and regions with depth discontinuities. One possible

solution is to use post-filtering [19] to align the disparity map edges with source image. This has been adopted here within OpenCV. Figure 3 compares the disparity map result, the upper row shows the results with stereoBM alone while the lower row shows the results with stereoBM and post-filtering.

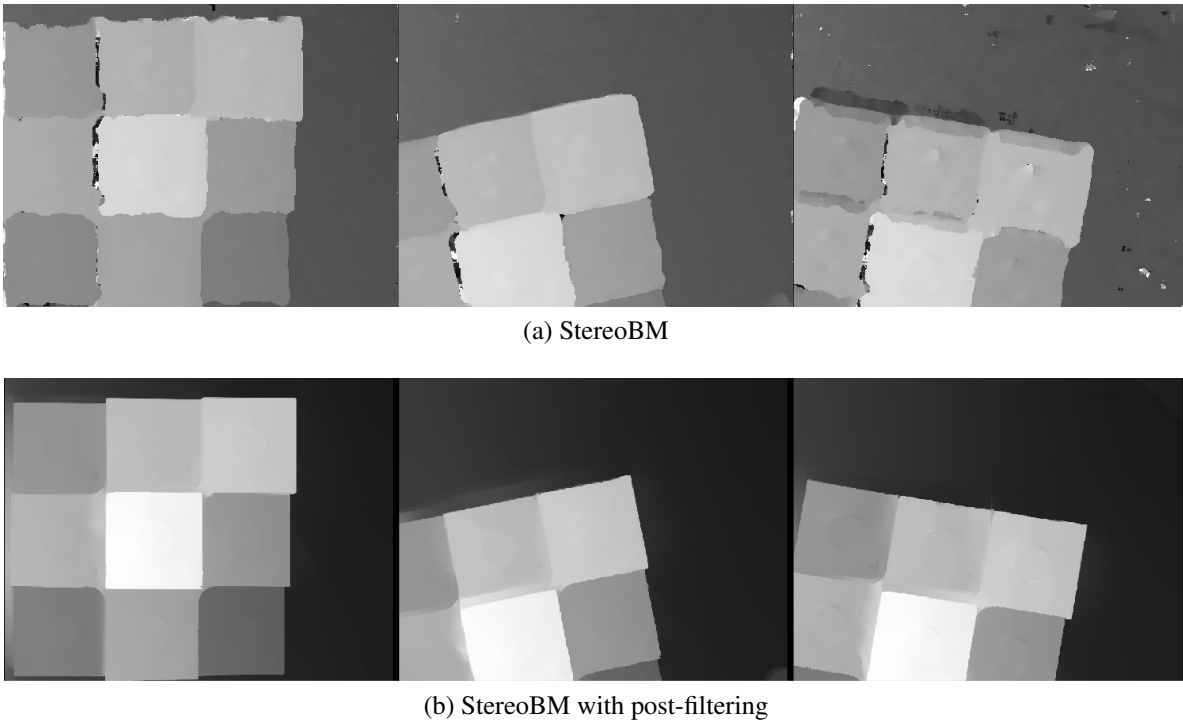


Fig 3: Compare the disparity map with and without post-filtering

### 2.3 Integrated system

Point cloud reconstruction from microscopic stereo-pair images requires several steps: camera calibration, image rectification, disparity computation, and 3D point cloud reconstruction. Each of these steps may require parameter adjustments to produce acceptable results. To facilitate the process and make it achievable by users that are not experts in computer vision, we have developed an interactive environment. This environment includes a GUI through which parameters can be adjusted using check-boxes, spin-boxes, and line-edit widgets. Intermediate and final results are

also shown. This GUI is written in C++ using Qt [20] and can be run on Windows and Linux platforms. We used the OpenCV library [18] for the computer vision algorithms, and the PCL library [21] was used to display and process point cloud data.

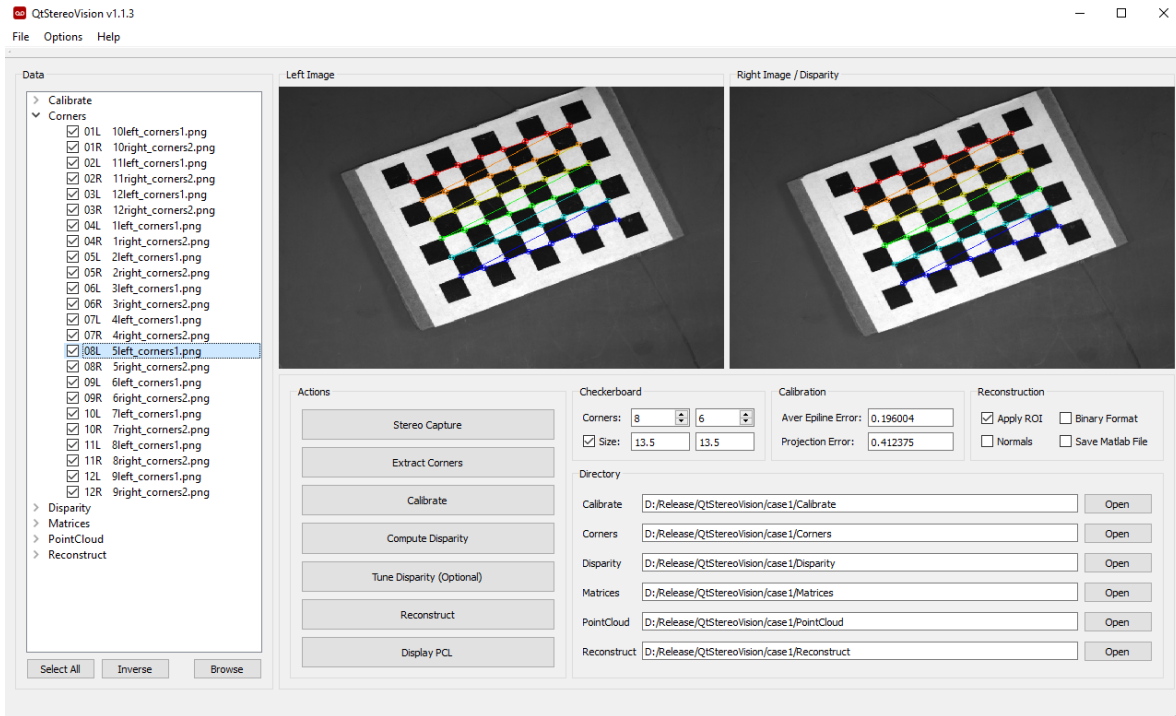
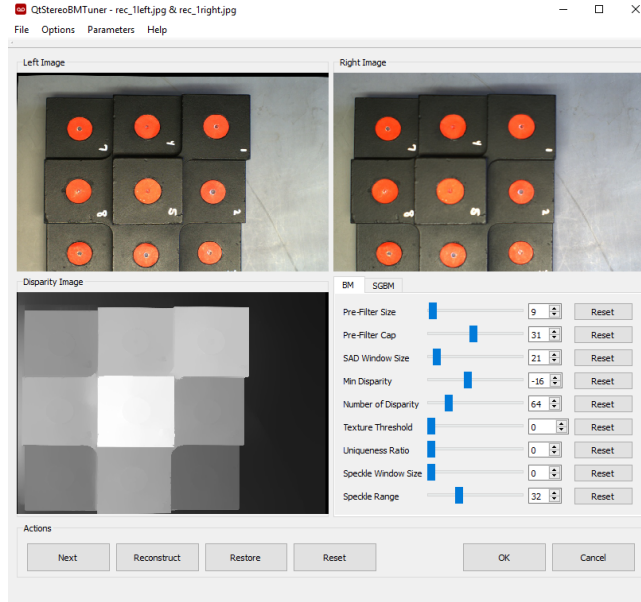
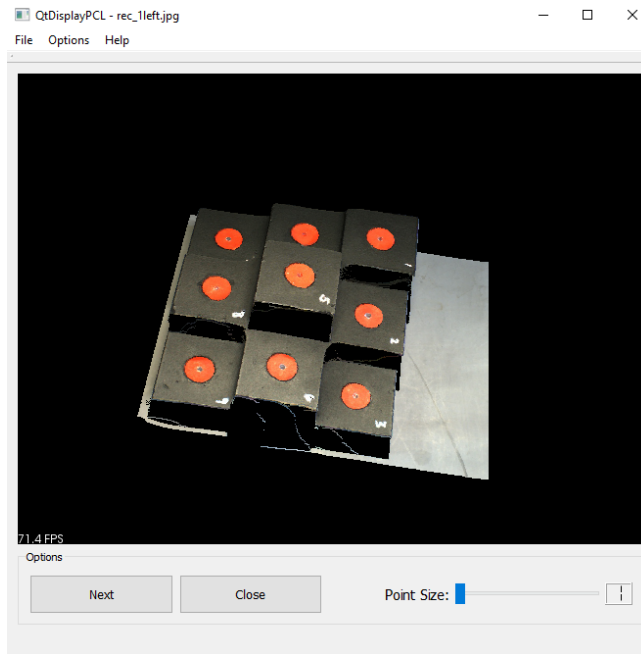


Fig 4: Integrated reconstruction software: main window

Figure 4 shows the main window of the software. On the left side of the interface is a tree-view structure used to select the input images, the output point clouds, as well as some intermediate results. Moving to the right, a display area facilitates visualization of the stereo-pair images (left and right), and the panel below contains the series of actions and options necessary to perform the point cloud reconstruction. The first step involves stereo capture of a calibration checkerboard pattern, and the user is guided through the process. The next step is the localization of the corners in the checkerboard images, and the calibration of the stereo cameras using the method described in [11].



(a) Disparity tuner panel



(b) Point cloud display

Fig 5: Integrated reconstruction software: (a) disparity tuner panel, and (b) point cloud display window

Once the calibration is complete, the output camera matrices are used to rectify left and right images. The disparity map can then be computed using either a block matching (BM) or a semi-global block matching (SGBM) algorithm [16]. Both BM and SGBM algorithms use nine param-

eters that can be adjusted. These can be adjusted using sliders while showing the disparity image produced by the current parameter values (see Fig. 5a). Once the disparity image computation is deemed acceptable by the user, the point cloud can be computed for each disparity image (see Fig. 5b). After computing the reconstruction [22], the display panel is invoked to immediately provide a visualization of the point clouds.

#### 2.4 Microscope tracking

Microscope tracking can be performed via the use of a rigidly attached optically tracked reference body, a calibration procedure to compute the transformation between the coordinate system specified by the rigid tracking body, and the coordinate system of the reconstructed stereo-pair point cloud [23]. We use a Polaris Spectra optical tracking system developed by Northern Digital, Inc. (Waterloo, Ontario, Canada) which has a reported tracking accuracy of 0.25-0.3mm RMS [24]. A commercially available rigid body reference with microscope mounting attachment (MICROSCOPE TRACKING ARRAY, Brainlab Inc., Westchester, IL) was employed to facilitate tracking of the surgical microscope.

The setup for microscope tracking calibration is sketched in Fig. 6 (a). To summarize, the goal of the microscope tracking calibration is to determine the rigid body transform that provides a mapping between the coordinate system of the reconstructed stereo-pair point cloud ( $X_{cam}$ ) and the coordinate system of the rigid body attached to the surgical microscope ( $X_{star}$ ). This calibration transform ( $T_{cam-star}$ ) is computed using a calibration phantom that is comprised of a series of fiducial disks that can be localized in both the reconstructed stereo-pair point cloud space and the coordinate system space of the microscope rigid body. The fiducial points are located in the reconstructed stereo-pair space via computation of disk centroids from the reconstructed point cloud.

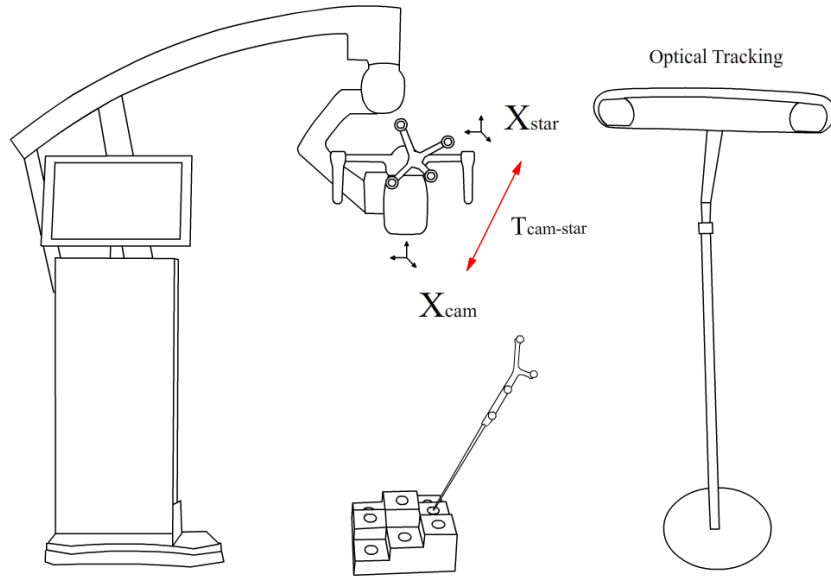
The fiducial point locations in the microscope rigid body space are determined via an optically tracked probe that can digitize the individual fiducial points relative to the microscope rigid body within the optical tracking system. Once these individual fiducial points have been localized in each space, a point-based registration [25] is computed to determine the camera calibration transform ( $T_{cam-star}$ ).

## 2.5 Validation experiments

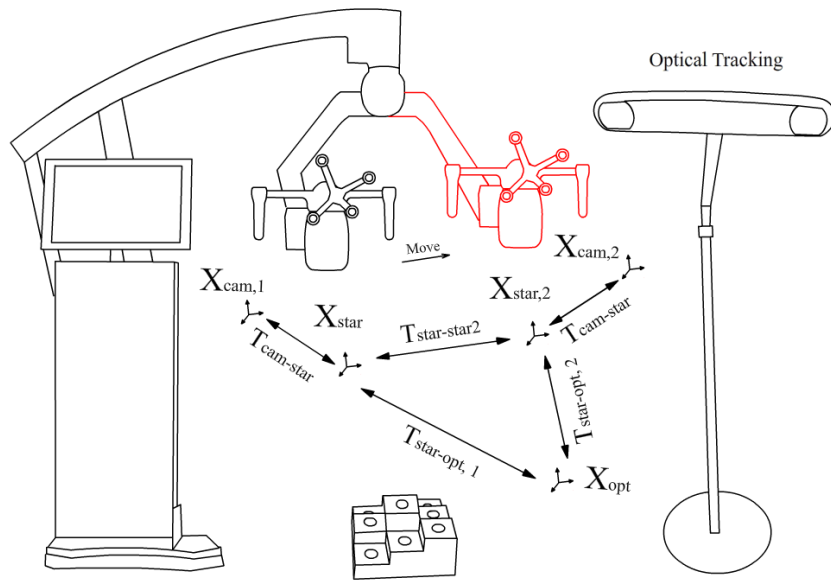
The validation experiment includes two parts: microscope tracking validation and vessel displacement validation. The aim of the microscope tracking validation is to ensure that the calibration transformation ( $T_{cam-star}$ ) is accurate via the transformation of a series of point cloud reconstructions, acquired at different microscope locations, to a reference coordinate space (see Fig. 6 (b)). At an initial position of the surgical microscope ( $X_{cam,1}$ ), the tracked location of the scanner was recorded ( $T_{star-opt,1}$ ), and a stereo-pair reconstruction was performed of the calibration phantom. With the phantom and optical tracking system in a fixed position, the surgical microscope was then moved to a second position ( $X_{cam,2}$ ). Again, the tracked location of the scanner was recorded ( $T_{star-opt,2}$ ), and a stereo-pair reconstruction was performed. Given the recorded data from the two locations, the fixed microscope calibration transformation ( $T_{cam-star}$ ) and the fixed optical tracking coordinate system ( $X_{opt}$ ), the stereo-pair reconstructed point clouds acquired at the two microscope locations can be transformed into the same space using the following equations:

$$X_{opt} = [T_{star \rightarrow opt,1}] [T_{cam \rightarrow star}] X_{cam,1} \quad (4)$$

$$X_{opt} = [T_{star \rightarrow opt,2}] [T_{cam \rightarrow star}] X_{cam,2} \quad (5)$$



(a) Calibration procedure



(b) Tracking experiment

Fig 6: The setup of calibration procedure and tracking experiment

The steps are as follows:

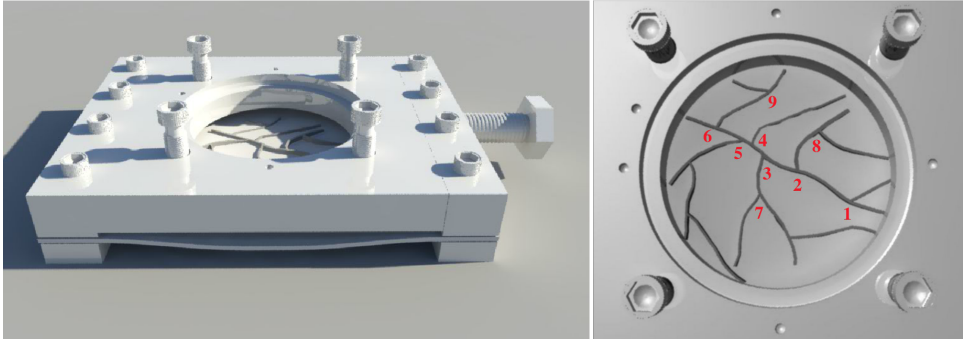
1. Place the scope at base position, then place the calibration phantom under the scope. Reconstruct the point cloud of the phantom.

2. Digitize the centroids of the nine disks and record the position of the scope using the optical tracking system. The transformation matrix can be computed.
3. Move the scope to another position, while keeping the phantom static. Reconstruct the phantom and record the scope position.
4. Repeat step 3.
5. Use the transformation matrix from step 2 to transform the point cloud in step 3 and 4 back to base position and then evaluate the error.

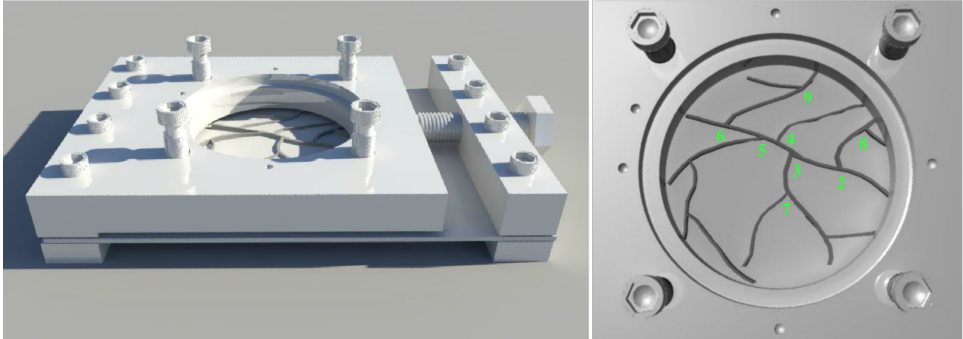
For the vessel displacement computation, we use the craniotomy device (described in section 2.1) to simulate brain shift via three states (baseline, stretch, and sag as shown in Fig. 7). The experimental steps are as follows:

1. Set the craniotomy device in the baseline state and place it under the scope.
2. Reconstruct 3D point cloud of the device and record the ground truth positions of vessel features marked on the membrane using optical tracking system.
3. Move the scope to a new position, and apply a 2 cm horizontal stretch (lateral shift) using the screw mechanism. Then repeat step 2.
4. Move the scope to another new position, and using the four screws around the craniotomy to displace the membrane downward by 1.6 cm (this simulates sag). Then repeat step 2.
5. Using the previous transformation matrix to transform point cloud in step 3 and step 4 to base space. The movement of features marked on the membrane can be computed after the application of the tracking transformations.

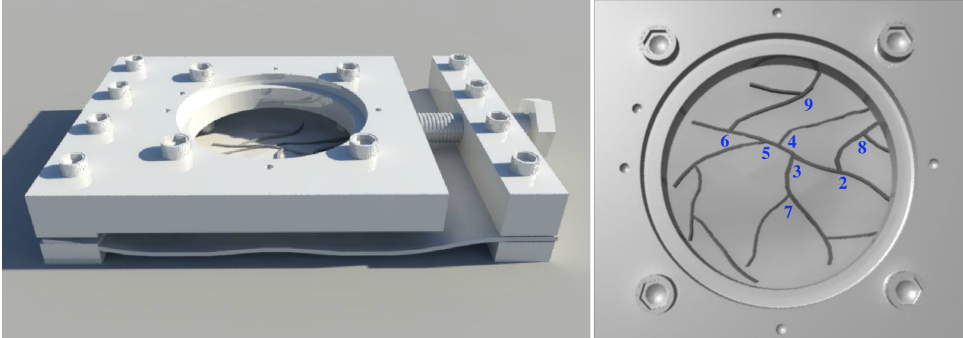
To validate our system, the deformations are recorded using the optically tracked stylus. This serves as the ground truth that can be subsequently compared to the tracked microscope stereo pair measurements.



(a) Baseline



(b) Stretch (Lateral Shift)



(c) Stretch + Sag

Fig 7: Three states of generating simulated brain shift: baseline, stretch (lateral shift), stretch as well as sag

### 3 RESULTS

Result for the stereo-pair camera calibration experiment are shown in the GUI (see Fig. 4). The average epiline error is 0.2 pixels, and the stereo projection error is reported as 0.41 pixels. Knowing the geometry of the calibration phantom, a reconstruction error of approximately 1 mm is estimated by systematically comparing the distance between nine divots. Since the microscope is tracked, the transformation between point clouds generated via scope acquisitions at different positions can be computed. We reconstructed the point cloud of the calibration phantom by moving the scope to three positions (see Fig. 8 (a) (b) (c)).

By applying the transformation matrix to the second and third point clouds (highlighted in yellow and blue, respectively, in Fig. 8), these two point clouds can be transformed into the same space as the initial point cloud (see Fig. 8 (d) (e)). Figure 8 (f) shows the results of registering all three point clouds together. The mean distance error is 0.64 mm in the x direction, 0.89 mm in the y direction, and 2.92 mm in the z direction. These errors are caused by reconstruction error and tracking error. The displacement is computed by registering the simulated vessel features on the simulated craniotomy device to the same space (baseline state) shown in Fig. 9. Note that feature No.1 is not included in the results because it is no longer visible following the stretch (lateral shift) operation of the craniotomy device, which can also happen in actual surgeries when part of the brain slides past the craniotomy. The difference between displacement in stereopsis (measured in 3D point cloud) and tracking system (ground truth) is calculated as displacement error and is found to be approximately 2 mm on average (see Fig. 10).

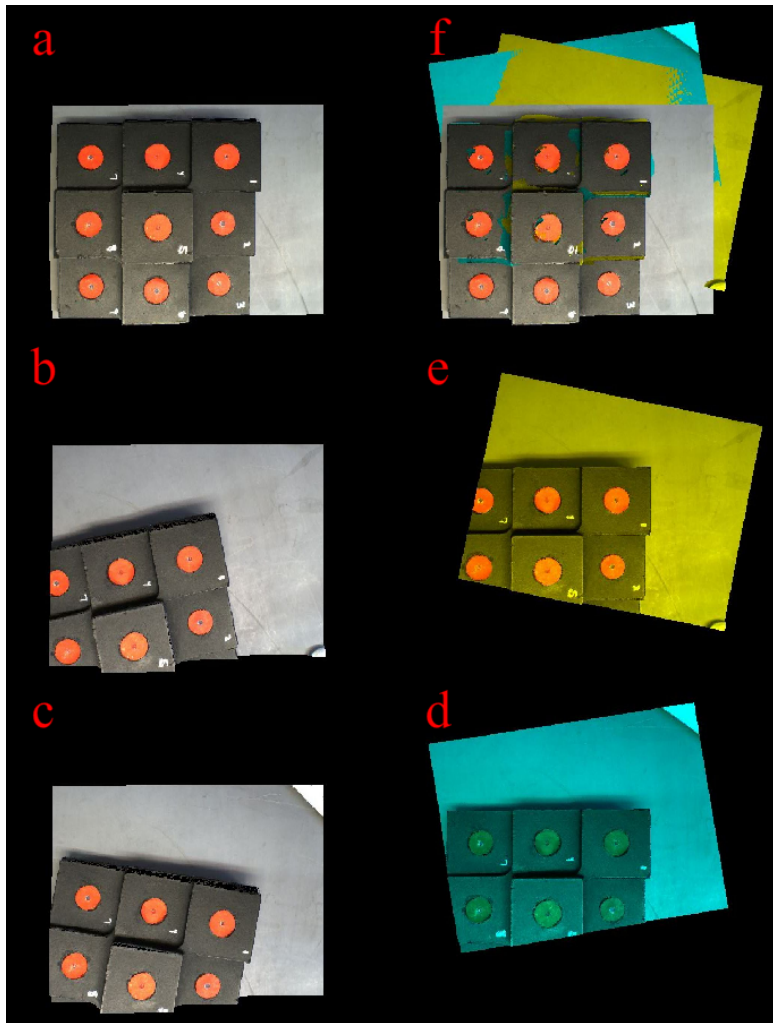


Fig 8: Registered point cloud reconstructed from different microscope position to same space

#### 4 DISCUSSIONS

The phantom experiments performed for the purpose of validating the tracking calibration for the surgical microscope yield a number of error metrics that provide some insight into the range of possible error sources that are contributing factors. These contributing factors include the error due to the stereo-pair reconstruction process, manual error associated with the fiducial digitization and centroid extraction, sub-optimal calibration phantom design and the tracking error associated with the rigid body attachment to the microscope and the tracked stylus.

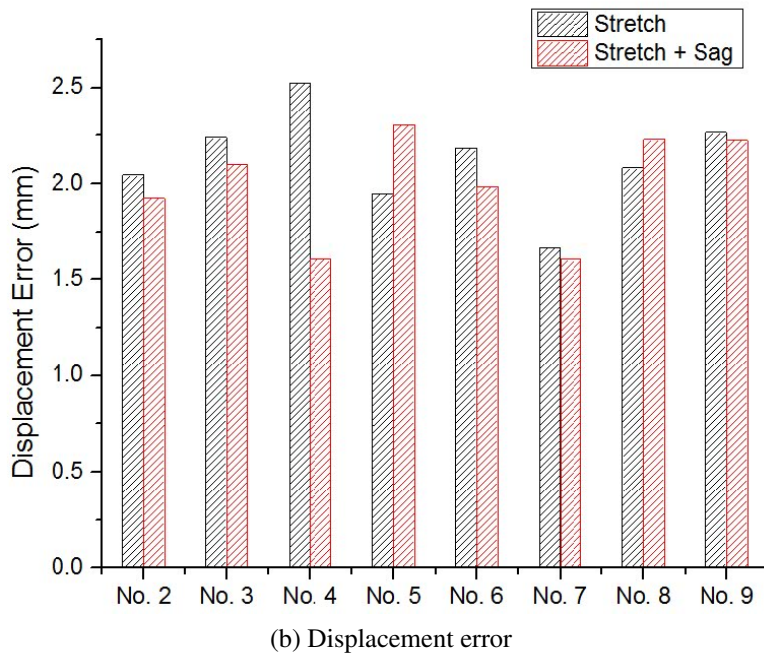
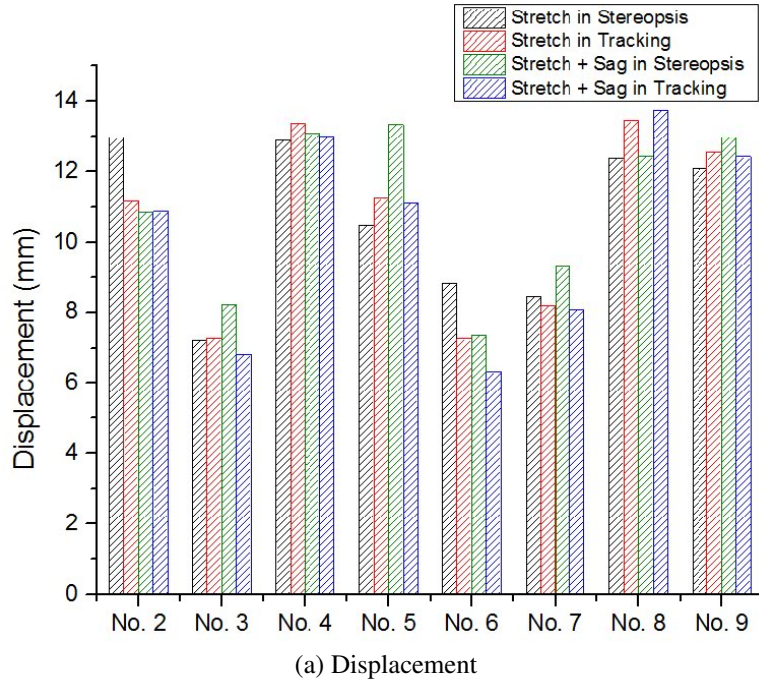


Fig 9: Bar of displacement and displacement error

The stereo-pair reconstruction error highly depends on the quality of the disparity computation. Camera calibration affects the rectification step, which is critical for computing disparity. The scope tracking error is computed by comparing the point clouds that are transformed to the same

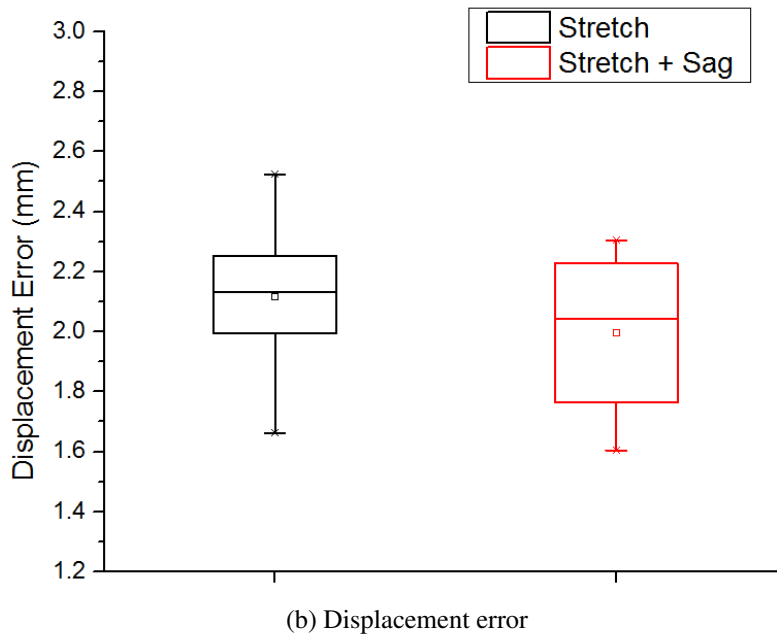
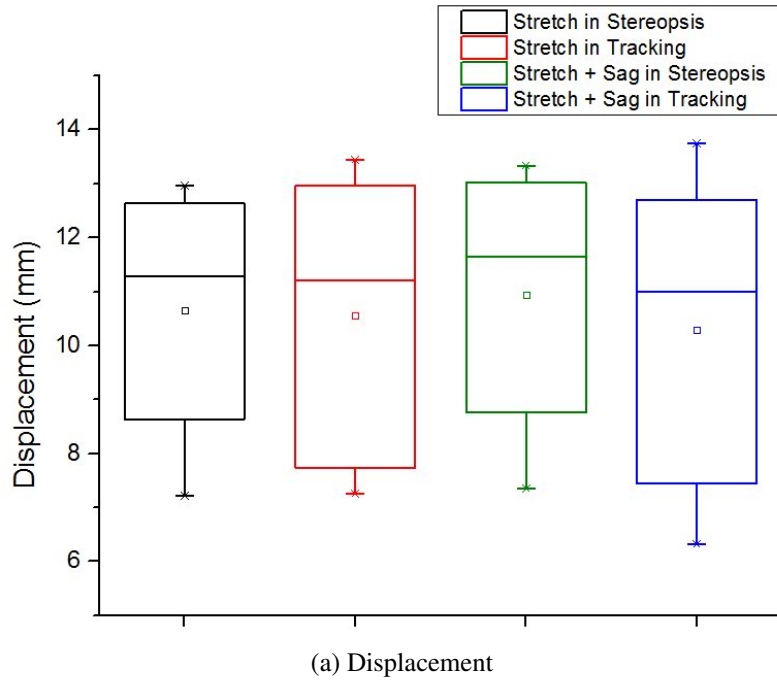


Fig 10: Box plot of displacement and displacement error

scope coordinates. The X, Y, and Z direction mean distance errors are computed and the results show that the error in the Z direction is higher than in the other two directions. This may be due to the error in estimating depth from disparity. The point cloud reconstruction is more accurate in the

horizontal direction than in the vertical direction. Considering that the maximum height difference of the steps on the phantom is nearly 50 mm (larger than the normally reported brain deformation), the mean distance error is, to some degree, acceptable. We also note that stereo reconstruction techniques are challenged by sharp edges such as the steps on the phantom. We expect that our reconstruction error would be smaller with a phantom that would have smoother edges as would the cortical surface.

Moreover, the error of the tracking system itself and the localization error associated with the use of a tracking stylus also contribute to the calibration error of the surgical microscope. Error associated with the tracking system used in these experiments are reported by the manufacturer and are within an acceptable range. However, any error associated with the calibration files generated for the tracking of the rigid body attached to the microscope as well as the tracked probe can be potential sources of error. Finally, any manual localization inaccuracy in the digitization of the points on the calibration phantom with the optically tracked probe can introduce errors.

The main goal of this work is to demonstrate the ability to take advantage of stereovision-based techniques to track tissue deformations with arbitrary movement of the surgical microscope. While the results presented indicate that the presented method of microscope tracking calibration is promising, there are a number of avenues for improving the calibration results. Primarily, refinement in reconstruction techniques should facilitate more accurate calibrations. Additionally, the use of an optimally designed calibration phantom would facilitate more accurate results as well. Finally, our calibration method is only useful for fixed microscope setting where the focal length and zoom factor cannot change during the whole procedure. Future methods will entail the ability to generate calibration data that allows the use of multiple microscope settings throughout the surgical procedure.

## 5 CONCLUSIONS

In this paper, we have proposed a GUI-based system that integrates all necessary functionality for reconstructing FOV of stereo-pair or microscope cameras including (1) capturing stereo-pair images or video streams, (2) extracting checkerboard corners, (3) calibrating stereo cameras, (4) computing disparity, and (5) displaying point clouds. Moreover, the parameters associated with the disparity computation can be modified in an interactive GUI to improve the results. This reconstruction system is functional, user-friendly, and it requires only minimal prior knowledge. By applying image-to-physical space registration, the stereoscopic microscope can be tracked, and freely moved without disrupting the surgical procedure. The reconstruction accuracy and displacement comparison results suggest that this system could be used to gather cortical data to measure and compensate for brain shift during image-guided surgery. This would extend the capability of conventional navigation system.

### *Disclosures*

No conflicts of interest including financial or others are declared by the authors.

### *Acknowledgments*

This work is funded by the National Institutes of Health, National Institute for Neurological Disorders and Stroke grant number R01-NS049251. We would like to acknowledge Zeiss, Inc., Point Grey Research, Inc., and Northern Digital, Inc. for providing essential equipment and resources, and John Fellenstein from the Vanderbilt Machine Shop for his assistance in our cortical surface deformation simulation device. We would also like to acknowledge Joselito Tiamson, Kim Robertson, and Carol Talbot for their assistance in using Pentero research microscope in an operating

room of Vanderbilt University Medical Center (VUMC) to apply our experiments.

### References

- 1 R. L. Galloway Jr, “The process and development of image-guided procedures,” *Annual Review of Biomedical Engineering* **3**(1), 83–108 (2001).
- 2 A. Nabavi, P. M. Black, D. T. Gering, *et al.*, “Serial intraoperative magnetic resonance imaging of brain shift,” *Neurosurgery* **48**(4), 787–798 (2001).
- 3 C. Nimsky, O. Ganslandt, S. Cerny, *et al.*, “Quantification of, visualization of, and compensation for brain shift using intraoperative magnetic resonance imaging,” *Neurosurgery* **47**(5), 1070–1080 (2000).
- 4 T. Gunnarsson, A. Theodorsson, P. Karlsson, *et al.*, “Mobile computerized tomography scanning in the neurosurgery intensive care unit: increase in patient safety and reduction of staff workload,” *Journal of neurosurgery* **93**(3), 432–436 (2000).
- 5 G. Unsgaard, O. Rygh, T. Selbekk, *et al.*, “Intra-operative 3d ultrasound in neurosurgery,” *Acta neurochirurgica* **148**(3), 235–253 (2006).
- 6 M. I. Miga, D. W. Roberts, F. E. Kennedy, *et al.*, “Modeling of retraction and resection for intraoperative updating of images,” *Neurosurgery* **49**(1), 75–85 (2001).
- 7 M. I. Miga, T. K. Sinha, D. M. Cash, *et al.*, “Cortical surface registration for image-guided neurosurgery using laser-range scanning,” *IEEE Transactions on medical Imaging* **22**(8), 973–985 (2003).
- 8 A. N. Kumar, M. I. Miga, T. S. Pheiffer, *et al.*, “Persistent and automatic intraoperative 3d digitization of surfaces under dynamic magnifications of an operating microscope,” *Medical image analysis* **19**(1), 30–45 (2015).

- 9 X. Yang, L. W. Clements, R. H. Conley, *et al.*, “A novel craniotomy simulation system for evaluation of stereo-pair reconstruction fidelity and tracking,” in *SPIE Medical Imaging*, 978612–978612, International Society for Optics and Photonics (2016).
- 10 X. Yang, “Stereo-pair Capture Software.” Vanderbilt.edu <https://my.vanderbilt.edu/xiaochen/archives/75>. (Accessed: August 2015).
- 11 Z. Zhang, “A flexible new technique for camera calibration,” *IEEE Transactions on pattern analysis and machine intelligence* **22**(11), 1330–1334 (2000).
- 12 R. I. Hartley, “Theory and practice of projective rectification,” *International Journal of Computer Vision* **35**(2), 115–127 (1999).
- 13 J.-Y. Bouguet, *Visual methods for three-dimensional modeling*. PhD thesis, Citeseer (1999).
- 14 K. Konolige, “Small vision systems: Hardware and implementation,” in *Robotics research*, 203–212, Springer (1998).
- 15 H. Hirschmuller, “Stereo processing by semiglobal matching and mutual information,” *IEEE Transactions on pattern analysis and machine intelligence* **30**(2), 328–341 (2008).
- 16 D. Scharstein and R. Szeliski, “A taxonomy and evaluation of dense two-frame stereo correspondence algorithms,” *International journal of computer vision* **47**(1-3), 7–42 (2002).
- 17 D. Scharstein and R. Szeliski, “Middlebury Stereo Evaluation - Version 3.” <http://vision.middlebury.edu/stereo/eval3/>. (Accessed: April 2017).
- 18 G. Bradski and A. Kaehler, *Learning OpenCV: Computer vision with the OpenCV library*, ” O’Reilly Media, Inc.” (2008).
- 19 OpenCV, “Disparity Map Post-filtering.” <http://docs.opencv.org/trunk/d3/>

- [d14/tutorial\\_ximgproc\\_disparity\\_filtering.html](#). (Accessed: April 2017).
- 20 “Qt Powerful, Interactive and Corss-Platform Applications.” <https://www.qt.io/>. (Accessed: July 2016).
- 21 “Point Cloud Library.” <http://www.pointclouds.org/>. (Accessed: July 2016).
- 22 R. Hartley and A. Zisserman, *Multiple view geometry in computer vision*, Cambridge university press (2003).
- 23 D. M. Cash, T. K. Sinha, W. C. Chapman, *et al.*, “Incorporation of a laser range scanner into image-guided liver surgery: Surface acquisition, registration, and tracking,” *Medical Physics* **30**(7), 1671–1682 (2003).
- 24 P. Spectra, “Polaris Optical Tracking System.” <http://www.ndigital.com/medical/products/polaris-family/>. (Accessed: July 2016).
- 25 M. Fitzpatrick, “Algorithms for Registration, Error Prediction, and Rotation Parameter Conversion in Matlab.” [http://eecs.vanderbilt.edu/people/mikefitzpatrick/computer%20programs/computer\\_algorithms\\_in\\_Matlab.htm](http://eecs.vanderbilt.edu/people/mikefitzpatrick/computer%20programs/computer_algorithms_in_Matlab.htm). (Accessed: July 2016).

**Xiaochen Yang** is currently a Ph.D. student in Computer Science, Vanderbilt University, USA. He received his bachelor’s and master’s degree in Chang’an University and University of Missouri-Columbia respectively. His research interests focus on image-guided surgery, computer vision and graphics, and 3D visualization and reconstruction. He is a student member of SPIE.

**Logan W. Clements** has been performing research in the field of image-guided surgery since 2002 and his primary research interests include intraoperative accuracy validation of surgical navigation

systems and the use of image-guidance technology to facilitate the adoption of minimally invasive techniques. He received his B.S., M.S., and Ph.D. in Biomedical Engineering from Vanderbilt University.

**Ma Luo** is currently a Ph.D. student in the Department of Biomedical Engineering at Vanderbilt University. He received his B.S. degree in Bioengineering from University of Pittsburgh in 2015. His research interests are in computational modeling and inverse problem for biomedical applications, particularly brain stimulation.

**Saramati Narasimhan** is currently a Ph.D. student in Biomedical Engineering at Vanderbilt University, Nashville, TN. She received her BS degree in Biomedical Engineering from the University of Miami. Her research interests focus on biomechanics, finite element modeling, and image-guided surgery. She is a student member of SPIE.

**Reid C. Thompson** is the Director of the Vanderbilt Brain Tumor Center, Nashville, TN, where he is also the Vice Chairman of the Department of Neurological Surgery. He is a neurosurgeon and clinician scientist with expertise in the surgical treatment of patients with complex brain and spinal cord tumors. He treats both adults and children and performs over 250 complex intracranial operations a year. His clinical practice includes the entire spectrum of brain tumors including low-grade gliomas, malignant gliomas, metastatic brain tumors, and benign tumors such as meningiomas and acoustic neuromas. In addition, he has special expertise in treating complex tumors involving the most critical parts of the brain such as the brain stem and skull base.

**Benoit M. Dawant** received the M.S.E.E. degree from the University of Louvain, Leuven, Belgium, in 1983, and the Ph.D. degree from the University of Houston, Houston, TX, in 1988. Since

1988, he has been on the faculty of the Electrical Engineering and Computer Science Department, Vanderbilt University, Nashville, TN, where he is a Cornelius Vanderbilt Professor and Professor of Electrical Engineering. He is also the Director of the Vanderbilt Institute for Surgery and Engineering and a Fellow of the IEEE. His main research interests include medical image processing and analysis. His current areas of interest include the development of algorithms and systems to assist in the placement of deep brain stimulators used for the treatment of Parkinsons disease and other movement disorders, the placement of cochlear implants used to treat hearing disorders, or the creation of radiation therapy plans for the treatment of cancer.

**Michael I. Miga** received his B.S. and M.S. from the University of Rhode Island in Mechanical Engineering in 1992, 1994, respectively. He received his Ph.D. from Dartmouth College in Biomedical Engineering in 1998. He joined the faculty at Vanderbilt University in the Spring of 2001 and is the Harvie Branscomb Professor at Vanderbilt. He is also a Professor of Biomedical Engineering, Radiology and Radiological Sciences, and Neurological Surgery. He is director of the Biomedical Modeling Laboratory, and co-founder of the Vanderbilt Institute for Surgery and Engineering (VISE). He is also a Fellow of the American Institute for Medical and Biological Engineering College. His research interests are in computational modeling and inverse problems for therapeutic applications and imaging.

## List of Figures

- 1 Surgical operating microscope with optical marker attached (a), optical tracking device (b), simulated craniotomy device (c), and calibration phantom (d)
- 2 Three pairs of stereo images placed at different positions with corner detected

- 3 Compare the disparity map with and without post-filtering
- 4 Integrated reconstruction software: main window
- 5 Integrated reconstruction software: disparity tuner panel, and point cloud display window
- 6 The setup of calibration procedure and tracking experiment
- 7 Three states of generating simulated brain shift: baseline, stretch (lateral shift), stretch as well as sag
- 8 Registered point cloud reconstructed from different microscope position to same space
- 9 Bar of displacement and displacement error
- 10 Box plot of displacement and displacement error

## **List of Tables**